This is the accepted manuscript made available via CHORUS. The article has been published as:

Foldover of nonlinear eigenmodes in magnetic thin film based feedback rings

P. A. Praveen Janantha, Boris Kalinikos, and Mingzhong Wu

Phys. Rev. B **95**, 064422 — Published 21 February 2017

DOI: 10.1103/PhysRevB.95.064422

Foldover of Nonlinear Eigenmodes in Magnetic Thin Film-Based Feedback Rings

P. A. Praveen Janantha,[1] Boris Kalinikos,[1,2] and Mingzhong Wu[1]†

[1]Department of Physics, Colorado State University, Fort Collins, CO 80523, USA
[2]St. Petersburg Electrotechnical University, 197376, St. Petersburg, Russia

Abstract: The foldover effect of nonlinear eigenmodes in feedback ring systems was observed for the first time. Experiments made use of a system that consisted of a magnetic thin film strip, which supported the propagation of spin waves, and a microwave amplifier, which amplified the signal from the output of the magnetic strip and then fed it back to the input of the magnetic strip. The signal amplitude vs. frequency response in this ring system showed resonant peaks which resulted from ring eigenmodes. With an increase in the resonance amplitude, those resonant peaks evolved from symmetric peaks to asymmetric ones and then folded over to higher frequencies. The experimental observations were reproduced by theoretical calculations that took into account the nonlinearity-produced frequency shift of the traveling spin waves.

Active feedback ring systems consisting of a closed loop of a dissipative transmission line and an active element to compensate for the dissipation constitute an excellent testbed for exploring nonlinear dynamics in driven damped systems. Example systems include electromagnetic transmission line ring oscillators [1,2,3,4], optical fiber rings [5,6,7,8,9], and magnetic thin film-based feedback rings [10,11,12,13,14]. Such systems not only sustain the self-generation of envelope solitons, both bright [1,6,7,11] and dark [15], but have also enabled the observation of symmetry-breaking nonlinear modes [11], chaotic solitons [2,7,8,13,14], and soliton fractals [12] and have also allowed for the study of the excitation of chaotic dynamics via different nonlinear processes [2,5,7,9,10,16,17].

This letter reports that active feedback rings also support another fascinating nonlinear effect - the foldover effect. The nonlinear foldover effect originates from the nonlinearity in which the oscillation frequency varies with the amplitude, and manifests itself as the bending of the resonant peak in an oscillation amplitude vs. frequency plot. It occurs in nonlinear systems as diverse as driven pendula [18], spring-based mechanical oscillators [19], electrical RLC resonant circuits [20], and precessional magnetic moments in both insulating and metallic magnets [21,22,23]. The effect, however, has never been observed in ring systems so far.

The experiments made use of an active feedback ring that consists of a magnetic thin film strip serving as a spin-wave transmission line and a microwave amplifier which amplifies the output signal from the magnetic strip and then feeds it back to the input of the magnetic strip. This ring system has a sequence of resonant eigenmodes for which the phase per round trip satisfies constructive interference conditions [24]. Thanks to these eigenmodes the amplitude vs. frequency response of the ring signal shows resonant peaks at certain frequencies, and these peaks fold over to higher frequencies when the peak amplitude is large. This foldover effect is intrinsic and originates from the nonlinearity-caused frequency shift of the traveling spin wave. It is not associated with either high-power heating or four-wave interactions, as evident from the experimental data. To better understand the physical origin of the observed foldover effect, theoretical calculations were carried out that took into account the nonlinearity of the spin waves. The theoretical results not only confirmed the experimental observations, but also showed the rolling over of the top part of the resonant peaks which cannot be measured experimentally.

Four important points should be highlighted. First, the foldover effects reported previously are associated with the nonlinearity-caused frequency shift of simple, local oscillations [18-23], while the foldover effect presented below results from the nonlinear frequency shift of waves traveling around a feedback ring. This indicates that the foldover effect not only occurs for local oscillations but also for traveling waves. Second, as mentioned above the active ring systems embrace rich nonlinear dynamics and have enabled the studies of a large number of new nonlinear phenomena [1-17]. The observation of the foldover effect presented below further demonstrates the excellent versatility of the feedback rings as a fundamental system for exploring nonlinear dynamics in general. Third, the foldover effect presented here should be universal and is expected to occur in any feedback ring systems, including electromagnetic transmission line oscillators [1-4] and optical fiber rings [5-9]. Future work that demonstrates the foldover phenomenon in these systems is of great interest. Finally, there is always a bi-stability phenomenon that accompanies the foldover effect, and such bi-stability can be used to develop intensity-dependent filters, power limiters, and switching devices [25,26]. The demonstration of the foldover effect in ring systems offers a new dimension for the development of these devices.

The ring setup is shown schematically in Fig. 1. It consists of a magnetic $Y_3Fe_5O_{12}$ (YIG) thin film strip and two microstrip transducers placed over the YIG strip for the excitation and detection of spin waves in the YIG strip. The YIG strip is magnetized by a perpendicular magnetic field. This film-field configuration supports the propagation of forward volume spin waves along the YIG strip and, at the same time, also prohibits three-wave nonlinear interactions [27,28]. The output signal from the detection transducer is fed back to the excitation transducer through an adjustable microwave attenuator and a microwave amplifier. The response in the ring is sampled through two directional couplers and is measured with a vector network analyzer. For the data presented below, the YIG strip was 1.6 mm wide and 55 mm long, the microstrip transducers were 50 μm wide and 2 mm long, the transducer separation (l) was held at 10.4 mm, and the magnetic field was 2990 Oe. Both the amplifier and the attenuator had a linear response over 1-8 GHz.

Figure 2 presents the characteristics of the YIG strip and the feedback ring. Figure 2(a) shows the transmission coefficient data ($\mathbf{S}_{21}$) measured as a function of frequency (f) for the transducer-YIG-transducer structure. The left diagram shows the amplitude vs. frequency response, namely, the amplitude of $\mathbf{S}_{21}(f)$. In the right diagram, the red curve presents the spin-wave dispersion curve determined from the phase of $\mathbf{S}_{21}(f)$, while the green curve shows a theoretical fit to the spin-wave dispersion equation [24,28]. To obtain the experimental dispersion curve, the spin-wave wavenumber $k(f)$ was calculated from the phase of experimental $\mathbf{S}_{21}(f)$, namely, $\phi(f)$, using the relation $\phi(f)=k(f)l+\phi_0$ where ϕ_0 is a phase constant and taking k=0 at the low cut-off frequency f=3.30 GHz of the transmission. The theoretical fit used [24,28]

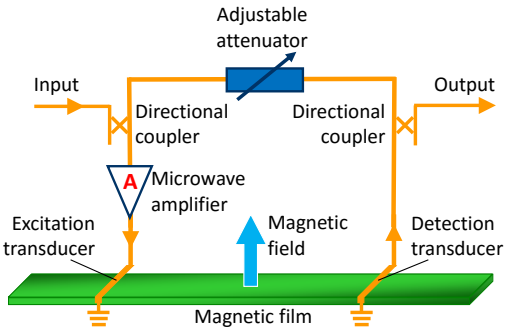

Fig. 1. Schematic of a magnetic thin film strip-based active feedback ring system.

$$\omega(k)=|\gamma|\sqrt{\left(H_0-4\pi M_s\right)\left(H_0-4\pi M_s\frac{1-e^{-kd}}{kd}\right)} \quad (1)$$

where ω=2πf is the frequency, $|\gamma|$ is the absolute gyromagnetic ratio, H_0 is the magnetic field, $4\pi M_s$ is the effective saturation induction of the YIG film, and d is the YIG film thickness.

The data indicate that the spin waves in the YIG film have a passband of about 3.30-3.65 GHz. The fitting used $|\gamma|$=2.8 MHz/Oe and $4\pi M_s$=1750 G. The fitting parameters were H_0 and d. For the fit given in Fig. 2(a), one has H_0=2920 Oe and d=10.2 μm. The field value is slightly smaller than the experimental value. Possible reasons for this difference include the errors in measuring H_0 and determining the low cut-off frequency of the spin wave and the assumption of zero anisotropy field in the YIG film. Note that for all the $\mathbf{S}_{21}$ measurements in this work, the signals from the vector network analyzer had the same power, which was -17 dBm.

Figure 2(b) shows the amplitude-frequency response and dispersion curve of the ring in the same format as in Fig. 2(a). Figure 2(c) presents the same data as in Fig. 2(b), but in much smaller frequency scales. One can see that in comparison with the transducer-YIG-transducer case, the amplitude-frequency response in the feedback ring exhibits a very similar passband but shows notable resonant peaks, while the dispersion curve shows steps at the frequencies of the resonant peaks. These peaks and steps are indicative of the ring eigenmodes [24]. The vertical dashed lines in Fig. 2(c) indicate the k values of the eigenmodes which were determined by the phase condition $kl+\phi_e=2\pi n$, where kl is the phase change due to the propagation of the spin wave, ϕ_e is the phase shift introduced by the electronic, and n is an integer and denotes the ring eigenmode index. Note that ϕ_e varies with f, and the ϕ_e value used in the k calculations ranged from 2.7 rad to 8.4 rad for n=1-25. It should be mentioned that when the attenuation (α) of the adjustable attenuator is relatively large and all ring eigenmodes experience an overall net loss (L) for one round trip, there is no spontaneous signal in the ring. However, if α is reduced to a certain level, the ring eigenmode with the lowest decay rate (n=5) can have a zero net loss, namely, L=0, and

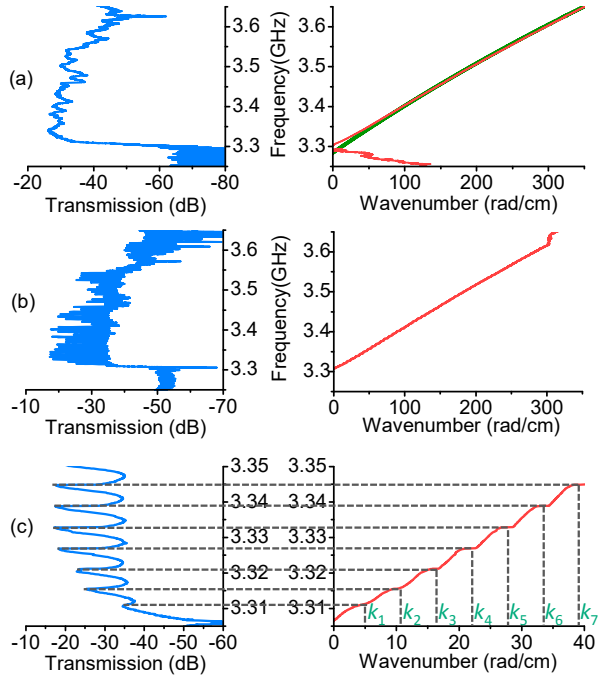

Fig. 2. (a) Transmission profile (left) and spin-wave dispersion curve (right, red) for a YIG strip. (b) Amplitude-frequency response (left) and spin-wave dispersion curve (right) for a YIG strip-based ring. (c) The same data as in (b) shown in smaller frequency scales. The green curve in (a) is a theoretical fit. The vertical dashed lines in (c) indicate the wavenumbers of the ring eigenmodes.

thereby start to self-generate in the ring. The data in Figs. 2(b) and 2(c) were taken at L=1.0 dB, at which there is no self-generation in the ring. Note that in the experiment one varies L by changing the attenuation of the attenuator. The larger the L is, the weaker the ring signal is.

Figure 3 presents the key results of this work. Figure 3(a) shows the effects of the ring net loss L on the amplitude-frequency response. The data show five ring resonant peaks, with the eigenmode index given in the top diagram. These peaks are similar to those shown in Fig. 2(c), but for a different frequency range. Figure 3(b) shows the resonant peak for the "n=21" eigenmode for three different L levels, as indicated. One can see that the "n=21" peak is almost perfectly symmetric at L=16.5 dB and L=8.5 dB, evolves to an asymmetric peak at L=3.5 dB, and folds over to the high-frequency side at L=2.0 dB and L=1.0 dB. Very similar behavior can also be seen for the "n=20" and "n=22" peaks. The "n=19" and "n=23" peaks, however, do not show the same foldover response. This is because these two modes have relatively lower amplitudes than the "n=20", "n=21", and "n=22" modes. They are relative weak because the loss at the corresponding frequencies are relatively high, as shown in Fig. 2(a), where the transmission profile is not flat mainly due to the frequency characteristics of the electronic components and possible reflections at the joints between different components in the feedback ring. These two modes did become stronger with a decrease in L, as shown in Fig. 3(a), but the resultant nonlinearity was still too weak to produce noticeable foldover responses. Although not shown, similar results are observed for the resonant peaks in other frequency ranges. These results together demonstrate the nonlinear foldover effect of the ring resonances.

The above-present foldover effect is associated with the nonlinearity-caused spin-wave frequency shift. Assuming $|u|^2$ as the power amplitude of the spin wave, one can write down the dispersion for the

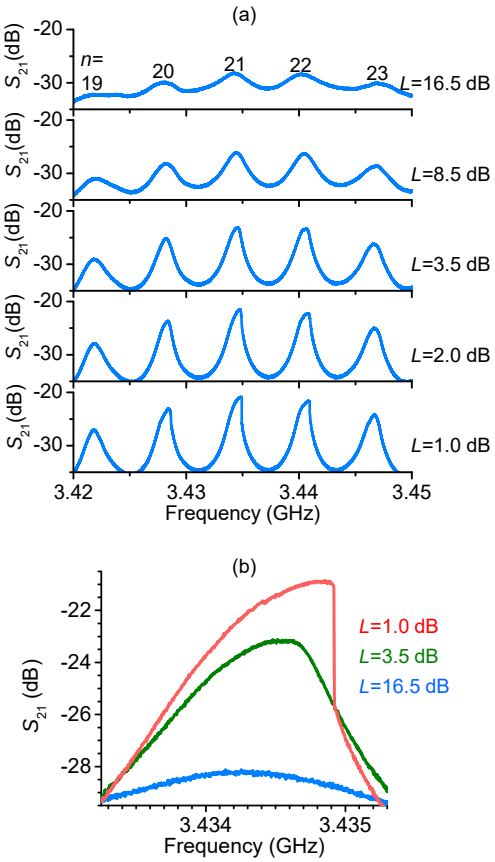

Fig. 3. Foldover of ring eigenmodes. (a) Ring amplitude-frequency responses measured at different ring overall net loss (L) levels. (b) Amplitude-frequency responses for the n=21 eigenmode measured at three L levels.

forward volume spin wave in the YIG strip as [24]

$$\omega\left(k,|u|^2\right)=|\gamma|\sqrt{\left[H_0-4\pi M_s\left(1-|u|^2\right)\right]\left[H_0-4\pi M_s\left(1-|u|^2\right)\frac{1-e^{-kd}}{kd}\right]} \tag{2}$$

Note that Eq. (2) reduces to Eq. (1) if one assumes $|u|^2=0$. The fitting of the experimental dispersion curve shown in Fig. 2(a) used Eq. (1), rather than Eq. (2). This is justified because during the measurements the input power was low and the spin wave was weak, resulting in $|u|^2<<1$. It is evident from Eq. (2) that for a given k, an increase in $|u|^2$ leads to an increase in ω. This means that if the amplitude of the ring resonant peak becomes large, the peak shifts to higher frequencies. As the top of the peak shifts more than the sides of the peak, the net effect is the bending of the peak to the high-frequency side, giving rise to the foldover behavior.

It is important to highlight that the foldover shown in Fig. 3 is towards the high-frequency side, but in principle it is also possible to have a foldover to the low-frequency side [18,20,23]. If one defines $N=\partial\omega/\partial\left(|u|^2\right)$ as the nonlinearity coefficient of a system, the sign of N dictates the direction of the foldover. Specifically, the resonant peaks fold towards the high-frequency side if $N>0$ and towards the low-frequency side if $N<0$. For the ring system shown in Fig. 1, one can flip the sign of N and thereby reverse the foldover direction simply by rotating the magnetic field to the film plane. For the in-plane configuration, the YIG strip supports backward volume spin waves for a field along the YIG strip length and surface spin waves for a field perpendicular to the strip length [27,28], both exhibiting $N<0$ [24].

To better understand the physics underlying the foldover effect in feedback ring systems, numerical calculations were carried out to reproduce the experimental observations. Referring to the system shown in Fig. 1 and considering a signal A_{in} input to the left directional coupler, after the signal passes through the amplifier and then the YIG strip, it appears at the output of the right directional coupler as

$$A_{\text{out}}=A_{\text{in}}\beta G\left[\eta_e\left(e^{ikl}e^{-\xi_{sw}l}\right)\eta_d\right]\beta \tag{3}$$

where β denotes the loss for the directional coupler to transfer a signal into or out of the ring and G is the gain provided by the amplifier. The square bracket term in Eq. (3) describes the change of the signal in the transducer-YIG-transducer structure, where η_{e} and η_{d} describe the attenuations due to the excitation and detection transducers, respectively, and ξ_{sw} denotes the spatial decay rate of the spin wave. For convenience, the term $\eta_e e^{-\xi_{sw}l}\eta_d$ is replaced by a single attenuation parameter η in the discussions that follow. A_{out} in Eq. (3) is only a small portion of the signal from the YIG strip due to the relatively large loss β, while the majority of the signal propagates to the attenuator and the amplifier and then back to the YIG strip. The net effect is the continuous circulation of the signal in the ring and a signal at the output of the right directional coupler as

$$A_{\text{out}}=\sum_{n=1}^{\infty}A_{\text{in}}\beta\left[G\eta e^{ikl}\right]^n\left[\left(1-\beta\right)\alpha\left(1-\beta\right)\right]^{n-1}\beta \tag{4}$$

where $(1-\beta)$ denotes the loss which the ring signal experiences every time it passes through the directional coupler, and α denotes the attenuation of the adjustable attenuator. From Eq. (4), one can define the complex ratio

$$\mathbf{S}_{21}=\frac{A_{\text{out}}}{A_{\text{in}}}=\sum_{n=1}^{\infty}\beta\left[G\eta e^{ikl}\right]^n\left[\left(1-\beta\right)\alpha\left(1-\beta\right)\right]^{n-1}\beta \tag{5}$$

Defining S_{21} as the amplitude of $\mathbf{S}_{21}$, $20\lg(S_{21})$ corresponds to the ring amplitude-frequency response measured in the experiment. From Eq. (5), one can write S_{21} as

$$S_{21}=\sqrt{\left[\sum_{n=1}^{\infty}\beta^2G^n\eta^n\left(1-\beta\right)^{2(n-1)}\alpha^{n-1}\cos(nkl)\right]^2+\left[\sum_{n=1}^{\infty}\beta^2G^n\eta^n\left(1-\beta\right)^{2(n-1)}\alpha^{n-1}\sin(nkl)\right]^2} \quad (6)$$

Equations (2) and (6) together allow for the calculation of the amplitude-frequency response in the ring.

For the theoretical results presented below, the calculations used β=0.15 (-16.5 dB), G=1.78 (45 dB), and α=-(L+7) dB, which are all experimental values. In order to have the frequency positions of the calculated resonant peaks match those of the experimental peaks, the calculations used l=11.3 mm, which is slightly larger than the actual transducer separation (10.4 nm). This adjustment was reasonable because the phase change (ϕ_e) due to the electrical circuit is not taken into account in Eqs. (4)-(6). Note that this phase change is much smaller than the change due to the spin-wave propagation (kl). The parameter η in Eq. (6) is frequency dependent and was determined using Eqs. (2) and (6) to fit the ring amplitude-frequency response measured at L=40 dB. The fitting assumed that $|u|^2$ was a constant ($|u_0|^2$) independent of ω. This assumption is justified because the amplitude-frequency response at L=40 dB is relatively flat and does not show interference patterns. Note that the "L=40 dB" amplitude-frequency response and its corresponding response in the k domain were used as a reference background in the calculations. The "S_{21} vs. ω" and "S_{21} vs. k" responses can be mapped to each other using Eq. (2).

The calculations involve the following steps. One first uses Eq. (6) to calculate the S_{21} vs. k response for a given L. Then, one obtains ($|u|^2$-$|u_0|^2$) as a function of k by examining the difference between the calculated S_{21} vs. k response with the background S_{21} vs. k response mentioned above. Next one uses the ($|u|^2$-$|u_0|^2$) vs. k response and Eq. (2) to calculate the corresponding ω vs. k response. By comparing the ω vs. k response with the S_{21} vs. k response, one finally obtains S_{21} as a function of ω for a particular L.

Figure 4 shows representative results. Figure 4(a) compares the calculated amplitude-frequency responses (red curves) with the experimental responses (blue curves) for three L levels, as indicated. Figure 4(b) shows the same red curve in the bottom diagram in (a), but in a much smaller frequency scale. It is evident that there is an almost perfect agreement between the experimental and calculated

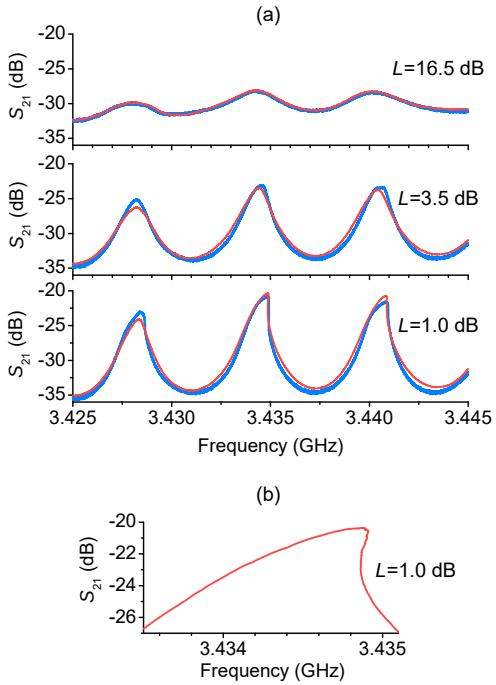

Fig. 4. Comparison of experiments and calculations. (a) Experimental (blue) and theoretical (red) ring amplitude-frequency responses for three different ring net loss (L) levels. (b) Calculated amplitude-frequency response for L=1.0 dB.

responses. What's more, the curve in Fig. 4(b) shows the rolling over of the top part of the peak, which is inherent but cannot be demonstrated experimentally. These results clearly justify the above-discussed physical origin of the foldover effect. Note that for the data shown in Fig. 3, the measurements were carried out by sweeping the frequency from low to high, and the amplitude jumped down from a high value to a lower value at the foldover. If the frequency is swept from high to low, it is expected that at the foldover the amplitude would jump up from a low value to a higher value at a frequency slightly lower than that for the down jump, resulting a hysteresis. This hysteresis response was not measured as the frequency sweeping direction was limited in the experiment. However, it is intrinsic [19,22,23] and can easily be imaged with the help of the foldover shown in Fig. 4(b).

In summary, the foldover effect was observed for nonlinear resonances in a YIG thin film strip-based active feedback ring. The amplitude vs. frequency response in the ring showed resonant peaks developed from ring eigenmodes. With an increase in the resonance amplitude, those resonant peaks evolved from symmetric peaks to asymmetric ones and then folded over to higher frequencies. To understand these results, theoretical calculations were carried out that took into account the nonlinearity of the spin waves. The calculated results almost perfectly agree with the experimental observations, confirming that the observed foldover effect originated from the nonlinearity-produced spin-wave frequency shift. The effect is not associated with either heating or the nonlinear parametric interactions of different spin waves, as evident by experimental data presented in the supplemental document. Finally, it should be noted that the foldover effect presented above differs from that observed previously for ferromagnetic resonance in magnetic thin films. In this work the foldover effect is associated with the nonlinear frequency shift of traveling spin waves, while in previous work the effect was for spatially uniform precessions of magnetic moments [21,22,23,25].

Acknowledgement: This work was supported in part by the U. S. National Science Foundation under Awards DMR-1407962 and ECCS-1231598; the U. S. Army Research Office under Award W911NF-14-1-0501; the SHINES, an Energy Frontier Research Center funded by the U.S. Department of Energy, Office of Science, Basic Energy Sciences under Award SC0012670; the C-SPIN, one of the SRC STARnet Centers sponsored by MARCO and DARPA; and the Russian Science Foundation under Award 14-12-01296.

†Corresponding author. E-mail: mwu@colostate.edu

[1] D. S. Ricketts, X. Li, and D. Ham, IEEE Trans. Microwave Theory Tech. **54**, 373 (2006).

[2] D. Ham, X. Li, and D. S. Ricketts, IEEE Commun. Mag. **44**, 126 (2006).

[3] D. S. Ricketts, X. Li, N. Sun, K. Woo, and D. Ham, IEEE J. Solid-State Circuits **42**, 1657 (2007).

[4] M. Ponton, A. Suarez, IEEE Trans. Microwave Theory Tech. **64**, 3499 (2014).

[5] L. Luo, T. J. Tee, and P. L. Chu, J. Opt. Soc. Am. B **15**, 972 (1998).

[6] J. M. Soto-Crespo, M. Grapinet, P. Grelu, and N. Akhmediev, Phys. Rev. E **70**, 066612 (2004).

[7] L. M. Zhao, D. Y. Tang, F. Lin, and B. Zhao, Opt. Commun. **252**, 167 (2005).

[8] L. M. Zhao, D. Y. Tang, and A. Q. Liu, Chaos **16**, 013128 (2006).

[9] F. Li, X. Feng, H. Zheng, C. Lu, H.Y. Tam, J. N. Kutz, and P.K.A. Wai, Opt. Commun. **284**, 2336 (2011).

[10] V. E. Demidov and N. G. Kovshikov, Tech. Phys. Lett. **24(4)**, 274 (1998).

[11] S. O. Demokritov, A. A. Serga, V. E. Demidov, B. Hillebrands, M. P. Kostylev, and B. A. Kalinikos, Nature **426**, 159 (2003).

[12] M. Wu, B. A. Kalinikos, L. D. Carr, and C. E. Patton, Phys. Rev. Lett. **96**, 187202 (2006).

[13] A. B. Ustinov, V. E. Demidov, A. V. Kondrashov, B. A. Kalinikos, and S. O. Demokritov, Phys. Rev. Lett. **106**, 017201 (2011).

[14] Z. Wang, A. Hagerstrom, J. Q. Anderson, W. Tong, M. Wu, L. D. Carr, R. Eykholt, and B. A. Kalinikos, Phys. Rev. Lett. **107**, 114102 (2011).

[15] B. A. Kalinikos, M. M. Scott, and C. E. Patton, Phys. Rev. Lett. **84**, 4697 (2000).

[16] A. M. Hagerstrom, W. Tong, M. Wu, B. A. Kalinikos, and R. Eykholt, Phys. Rev. Lett. **102**, 207202 (2009).

[17] M. Wu, A. M. Hagerstrom, R. Eykholt, A. Kondrashov, and B. A. Kalinikos Phys. Rev. Lett. **102**, 237203 (2009).

[18] Y. Xu, T. J. Alexander, H. Sidhu, and P. G. Kevrekidis. Phys. Rev. E **90**, 042921 (2014)

[19] Donoso, Guillermo, and Celso L. Ladera. Eur. J. of Phys **33**, 1486 (2012).

[20] B. Cretin and D. Vernier. E-print: arxiv.org/abs/0801.1301 (2008).

[21] M. T. Weiss. Phys. Rev. Lett. **1**, 239 (1958).

[22] J. Lustikova, Y. Shiomi, Y. Handa, and E. Saitoh. J. Appl. Phys. **117**, 073901 (2015).

[23] Y. S. Gui, A. Wirthmann, N. Mecking, and C.M. Hu Phys. Rev. B **80**, 060402 (2009).

[24] M. Wu, in *Solid State Physics*, edited by R. Camley and R. Stamps (Academic Press, Burlington, MA, 2011), vol. 62, pp. 163–224.

[25] Y. K. Fetisov, C. E. Patton, and V. T. Synogach, IEEE Trans. Magn. **35**, 4511 (1999).

[26] D. Zhang, M. Trepanier, O. Mukhanov, and S. M. Anlage, Phys. Rev. X **5**, 041045 (2015).

[27] P. Kabos and V. S. Stalmachov, *Magnetostatic Waves and Their Applications* (Chapman and Hall, London, UK, 1994).

[28] D. D. Stancil and A. Prabhakar, *Spin Waves – Theory and Applications* (Springer, New York, 2009).